

## ENT637 Case Study Report Cover Sheet.

### Module Details

Module Name: Individual Case Study      Module No: ENT637

Case Study Title: Structural Health Monitoring of Offshore Wind Turbines

Supervisor: Professor Rhys Pullin

### Personal Details

Name: Tobias Tilsed      Student No: 24109092

Degree: MSc Advanced Mechanical Engineering

### Declaration

I hereby declare that, except where I have made clear and full reference to the work of others, this submission, and all the material (e.g. text, pictures, diagrams) contained in it, is my own work, has not previously been submitted for assessment, and I have not knowingly allowed it to be copied by another student. In the case of group projects, the contribution of group members has been appropriately quantified.

I understand that deceiving, or attempting to deceive, examiners by passing off the work of another as my own is plagiarism. I also understand that plagiarising another's work, or knowingly allowing another student to plagiarise from my work, is against University Regulations and that doing so will result in loss of marks and disciplinary proceedings. I understand and agree that the University's plagiarism software 'Turnitin' may be used to check the originality of the submitted coursework.

Signed:



Date:

3<sup>rd</sup> May 2025

---

# Structural Health Monitoring of Jacket Foundations in Offshore Wind Turbines

---

School of Engineering  
Cardiff University  
Queen's Buildings  
14 - 17 The Parade  
Cardiff  
CF24 3AA

**Candidate:** Tobias Tilsed (24109092)

**Programme:** MSc Advanced Mechanical Engineering 2024 /25

**Project Supervisor:** Professor Rhys Pullin



---

ABSTRACT.....	1
INTRODUCTION.....	1
<b>CHAPTER 1: CLIMATE CHANGE.....</b>	<b>2</b>
<b>CHAPTER 2: WIND MAPS UK.....</b>	<b>5</b>
<b>CHAPTER 3: COMPONENTS OF AN OFFSHORE WIND TURBINE.....</b>	<b>10</b>
<b>CHAPTER 4: FOUNDATION TYPES.....</b>	<b>12</b>
<b>CHAPTER 5: MODES OF CONDITION MONITORING.....</b>	<b>14</b>
<b>CHAPTER 6: TYPICAL FAILURE IN JACKET FOUNDATIONS.....</b>	<b>16</b>
<b>CHAPTER 7: VIBRATIONAL ANALYSIS OF JACKET FOUNDATIONS.....</b>	<b>21</b>
<b>CHAPTER 8: THE ECONOMIC IMPACT OF FAILURE.....</b>	<b>32</b>
<b>CHAPTER 9: EXISTING PROJECT WORK.....</b>	<b>35</b>
<b>CHAPTER 10: ROADMAP FOR SUMMER.....</b>	<b>38</b>
CONCLUSION.....	40
REFERENCES	
APPENDIX	

---

---

## ABSTRACT

---

This report examines the scientific understanding of anthropogenic climate change, with a particular focus on projected sea level rise and its implications for energy infrastructure. This sets the context for a technical exploration of offshore wind turbines as a more sustainable alternative to hydrocarbon-based power generation. The report begins with an analysis of wind resources in UK waters, identifying viable installation zones based on bathymetry and wind velocity. The structural and electrical components of modern offshore wind turbines are then outlined, alongside a comparison of monopile and jacket foundation types. The paper reviews condition monitoring methods, with an emphasis on vibrational analysis and the use of accelerometers in jacket foundations. Typical failure modes are categorised, and a critical review of machine learning algorithms applied to experimental vibration data is presented. Economic justifications for predictive maintenance are evaluated, highlighting its role in both risk mitigation and investor confidence. Finally, this report sets the stage for the author's upcoming experimental study, which builds upon a prior student project, with an explicit plan to expand its scope and analytical rigor.

---

## INTRODUCTION

---

The design-stage optimisation of offshore wind turbine infrastructure has been the focus of several generations of engineers - particularly over the last 30 years. As a result, today's turbines are robust, efficient, and capable of long-term deployment in extreme offshore environments. Yet, despite these advances, operational degradation remains unavoidable. Materials fatigue, corrosion, and environmental stresses accumulate over time and can lead to sudden, catastrophic failure if left unmonitored. At this point in history, the challenge is no longer to eliminate failure entirely, but to develop affordable and reliable methods for detecting emerging degradation in real time. This enables the selective replacement of defective components where possible - or, failing that, the preservation of healthy subsystems before a full-system collapse occurs. This report

focuses on offshore wind turbine jacket foundations, where subtle vibrational changes can serve as early indicators of structural damage. By understanding these dynamic signatures and linking them to specific failure modes, it becomes possible to intervene intelligently - reducing downtime, preserving safety, and ultimately protecting the viability of offshore wind as a cornerstone of the UK's decarbonised energy future.

---

## CHAPTER 1: CLIMATE CHANGE

---

There are two major ice sheets in today's global topography: Greenland and Antarctica (Otosaka et al 2023). These have accumulated in volume over long periods of time - three and thirty four million years, respectively (Christ et al 2021; Galeotti et al 2016). This is because, during this time, the snow in these regions has not thawed or runoff (Seo et al 2015).

The volume of the Greenland ice sheet is  $2.96 \times 10^{15} (m^3)$  (Bamber et al 2013); the volume of the Antarctic ice sheet is  $27.0 \times 10^{15} (m^3)$  (Fretwell et al 2013). This means that the latter has 9.12 times the volume of the former. These volumes were meticulously determined via radar sounding - which uses the time taken for impulses of photons to be transmitted from the surface, travel through the ice, reflect off of the bedrock surface, and return to the sensor at the surface of the ice to determine its depth.

78% of the Greenland volume exists above sea level (Bamber et al 2013); with this being 60% for the Antarctic volume (Gasson et al 2020). This means that there is  $2.31 \times 10^{15} (m^3)$  - Greenland – and  $16.2 \times 10^{15} (m^3)$  - Antarctic - of ice above sea level. These asymptotically translate into discrete increases in global sea height of 7.36 (m) (Morlighem et al 2016) - Greenland – and 58.0 (m) (Fretwell et al 2013) - Antarctic. This makes the combined potential sea level rise 65.36 (m).

If the sea level were to rise by this maximum change in height - the UK topography would transform into that outlined in Figure 1 below. This would necessitate a huge sociological transformation - mass internal migration (Lincke et al 2021) - and a radical expansion of the elevated built environment. To extend the time before this is required, it is essential to reduce - and in the ideal case, eliminate - the net annual loss of ice in both the Greenland and Antarctic volumes.

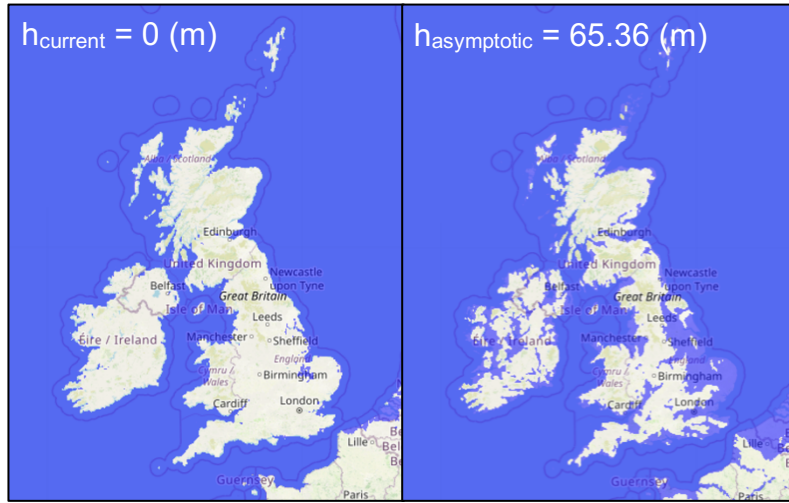


Figure 1: current boundary between land and sea versus that after complete melting of the Greenland and Antarctic volumes (FloodMap 2025).

The data for volume loss each year at both the Antarctic and Greenland ice sheets is shown in Table 1 of the Appendix. These data were collected via measuring the change in the gravitational force through time. As the ice melts and the mass hence redistributes, the size of the gravitational force acting at a fixed point at some distance away from earth will vary by an exceedingly small but nonetheless measurable quantity.

One major strategy in reducing the annual melt volume of both the Greenland and the Antarctic ice sheets is to change the method of power generation in the UK. Power generation that relies on the combustion of hydrocarbons releases carbon dioxide into the atmosphere; this increases heat globally despite the sun outputting the same power due to the greenhouse effect (Wijngaarden and Happer 2020).

Governments around the world engaged with the United Nations Framework Convention on Climate Change in 1992 (Hermwille et al 2015). While this didn't stipulate precise targets and metrics, it laid the ideological foundations for the subsequent conventions that would. Namely, in 1997, the Kyoto agreement in Japan was committed to by 197 countries. For the first phase of the commitment, developed nations - termed Annex I countries - were required to reduce their greenhouse gas emissions by 5.2% below 1990 levels; this was to be achieved between the years 2008 and 2012 (Grunewald and Martinez-Zarzoso 2015). For the second phase of the commitment, developed nations were required to reduce their emissions by 18% below 1990 levels; this was to be achieved between 2013 and 2020.

Subsequent to the Kyoto agreement, in 2015, 195 countries adopted the Paris agreement. This didn't set the same quantified and legally binding mandates of reduction in  $CO_2$  as Kyoto; instead - the Paris agreement emphasised the need for the rise in global temperature to remain under  $1.5^{\circ}C$  (Falkner 2016).

In 2019, the UK Government set national targets of a reduction in greenhouse gas emissions of 68% by 2030; 81% by 2035 and 100% - Net Zero - by 2050. As shown in Figure 31 of the Appendix, the UK has made sustained progress between 2012 and 2024 in reducing the proportion of the supply that is hydrocarbon based and in increasing the proportion that is renewable (Morley 2025). On 30th September 2024, the UK's final coal fired power generation facility - Ratcliffe on Soar - ceased generation.

Therefore, as UK offshore wind assets increasingly take the place of the hydrocarbon modes of power generation that are being phased out, it is imperative that this technology is well understood, and that any predictive maintenance is sufficiently mapped prior to full scale deployment.

---

## CHAPTER 2: WIND MAPS UK

---

When contemplating the power available for extraction via rotating the shaft of the generator in a wind turbine it is crucial to reflect on Equation 1 (Okulov and Sorensøn 2010):

*Equation 1:* 
$$P_{extractable} = \frac{1}{2} \cdot \rho \cdot A \cdot v^3 \cdot C_P \cdot \eta_M$$

$$(W) = (\text{unity}) \left( \frac{kg}{m^3} \right) (m^2) \left( \frac{m}{s} \right)^3 (\text{unity})(\text{unity})$$

Where  $C_P$  represents the power coefficient – typically between 0.45 and 0.50 for modern turbines; where this asymptotes theoretically at 0.593 - the Betz limit (Dehtyriov et al 2021). Where  $\eta_M$  represents the efficiency term of the generator itself – the heat loss via electromagnetic flux – typically between 0.90 and 0.97 for modern generators (Bašić et al 2019). What this means is that the extractable power available scales nonlinearly with the wind speed - the only meaningfully variable term for any given design.

It is useful to bear in mind that modern turbines are designed to cease generation when winds exceed an upper limit for  $v$  of typically  $25 \left( \frac{m}{s} \right)$  – known as the cut out speed – and that typically any wind speed below  $3 \left( \frac{m}{s} \right)$  will not transmit sufficient torque – the cut in speed (Wang et al 2021).

In 2015, researchers at the Technical University of Denmark published a global database - known as the Global Wind Atlas - of mean average wind speeds and their associated power (Gruber et al 2021). This database was generated via simulation and validated through sampling. The data extend 200 (km) beyond the land-coast boundary. Figure 32 of the Appendix shows a colourmap visualisation of this mean average wind

speed, globally; Figure 33 of the Appendix refines this visualisation by constraining the sea depth to  $5 \leq d_{sea} \leq 50$  (m).

These limits were chosen as Monopile foundations are typically used for sea depths of  $20 \leq d_{sea} \leq 40$  (m) with Jacket foundations being used for sea depths of  $5 \leq d_{sea} \leq 50$  (m) (Wu et al 2019). Sea depths beyond this necessitate floating turbines that are tied to the seabed through cables; this is a significantly less mature technology. In 2023, only 231.4 (MW) of the 68,300 (MW) global installed capacity – just 0.339% – used the Floating technology (McCoy et al 2024).

What Figure 33 demonstrates is that the seabed to the East of England and that of West Alaska are the two largest areas of high velocity wind with an appropriate sea depth for Monopile or Jacket foundation use. Figure 2, below, provides a detailed visualisation of this wind speed about the UK – separating the sea depths for Monopile; Jacket; Floating, respectively.

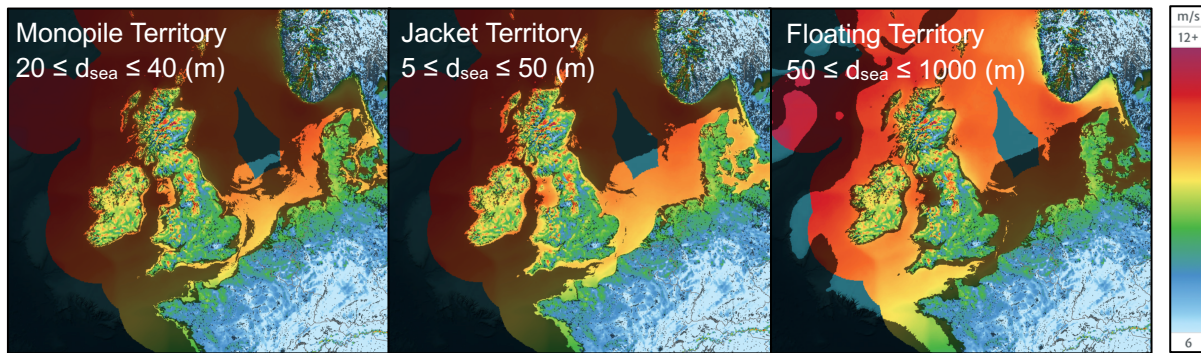


Figure 2: visualising mean wind speed about the UK with respect to the bounds of sea depth associated with each foundation technology (Global Wind Atlas 2025).

What this reveals are significant regions of eligible sea depth and wind velocity for all three technology types – with wind speed generally increasing slightly as the water becomes deeper.

Figure 34 of the Appendix visualises the locations of the current offshore assets with nation state boundaries; Figure 35 of the Appendix combines these asset locations with the wind speed visualisations of Figure 3 for:  $5 \leq d_{sea} \leq 50$  (m).

Taking the broad area to the East of England – including regions of sea that belong to France, Belgium, the Netherlands, Germany, Denmark, Norway; then taking a polygonal sample of this region that falls within the  $5 \leq d_{sea} \leq 50$  (m) constraint – a sample with a projected area of 135,588 ( $km^2$ ) is found, observed below in Figure 3.

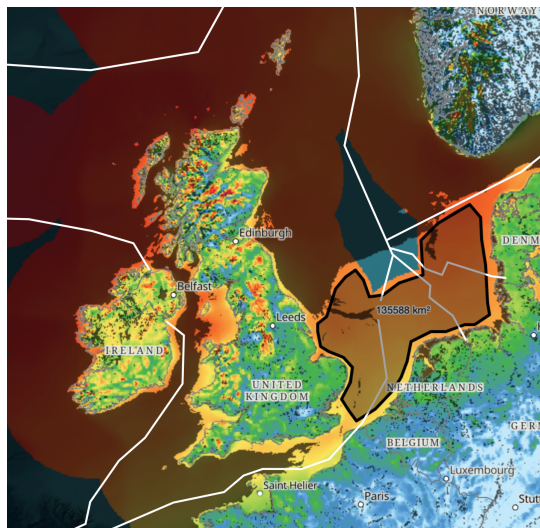


Figure 3: analysing a significant sample of the viable domain (Global Wind Atlas 2025)

This is equivalent to a square with side length 368 223 (m). The following analysis will use the SWT-7.0-154 turbine for reference as this is the most prevalent model currently installed in the UK.

Taking a downwind spacing of  $10 \cdot D_{rotor}$  and a lateral spacing of  $4 \cdot D_{rotor}$  (Denholm et al 2009) the representative configuration detailed in Figure 36 of the Appendix is arrived at. These geometries have been determined to be maximally efficient – if turbines are installed closer to each other than this, the volumetric flow of the air does not have sufficient distance to redistribute towards uniformity between turbines and its usable momentum and consequential extractable power would be reduced.

This forms a projected area per unit turbine of  $948\ 640 \left(\frac{m^2}{turbine}\right)$ . With a sample area of  $135\ 588\ 000\ 000\ (m^2)$  this would allow for 142 929 unique turbines – Calculation 1 of the Appendix.

Taking  $v = 10.04 \left(\frac{m}{s}\right)$  from Figure 37 of the Appendix and using this with Equation 1 as per Calculation 2 of the Appendix it is found that each turbine – idealising for uniform mean wind speed throughout the full sample - would generate **4.94 (MW)**. This means that the sample outlined in Figure 3 would, if fully populated and in typical conditions, output: **705.50 (GW)** of power.

For context, the typical electricity demand of the United Kingdom is on the order of **33 (GW)** – where this varies quite substantially between around 20 (GW) and 45 (GW) depending on the time of day and the outside temperature (Morley 2025). The typical instantaneous worldwide demand for electricity is around **3250 (GW)** (World Bank 2025).

This means that the sample would – if fully populated and in typical conditions – output approximately **21.38** times the typical demand of the United Kingdom and **21.71 %** of the Global electricity demand.

The frequency of the output alternating current power remains at 50 Hz at the point that it is supplied to the grid (Ma et al 2017) despite the variable wind speed and hence variable rotational velocity of the generator shaft. This is achieved via a sophisticated manipulation of the output power from:

$$AC [\neq 50\ Hz] \rightarrow DC [no\ frequency] \rightarrow AC [50\ Hz]$$

The rectification stage - AC → DC - has an efficiency of  $0.97 \leq \eta_{rect} \leq 0.99$ ; the inversion stage - DC → AC - has an efficiency of  $0.96 \leq \eta_{inv} \leq 0.98$ . Typical frequencies of the AC directly post generation are  $1 \leq f_{preconversion} \leq 5\ (Hz)$ .

It is worth noting that the power output associated with offshore wind is inherently variable through time, independent of demand. This is because - as per Equation 1 - the extractable power is a function of the wind velocity; that there is natural variability in this wind velocity through time at any given offshore location (Bakhoday-Paskyabi et al 2022).

The distribution of wind speed through time in a fixed location can be shown to be sufficiently represented by the Weibull distribution (Azad et al 2019), where (Wadi and Elmasry 2021):

$$Equation\ 2:\quad y_1(x) = \frac{k}{c} \cdot \left(\frac{x}{c}\right)^{(k-1)} \cdot e^{-(\frac{x}{c})^k} \quad [Weibull\ PDF]$$

$$Equation\ 3:\quad y_2(x) = 1 - e^{-(\frac{x}{c})^k} \quad [Weibull\ CDF]$$

$$Equation\ 4:\quad c = \frac{v_{mean}}{\Gamma(1 + \frac{1}{k})}$$

$$and:\quad 1.9 \leq k_{typical,offshore} \leq 2.5$$

Figure 38 of the Appendix shows the typical emergent organisation of average types in a positively skewed Weibull distribution. Taking  $k = 2.1$  and recalling from Figure 37 that  $v_{mean} = 10.04 (\frac{m}{s})$ ,  $c$  is observed to be  $11.3358 (\frac{m}{s})$  as per Calculation 6 of the Appendix. These magnitudes of  $k = 2.1$  and  $c = 11.3358 (\frac{m}{s})$  give rise to the PDF and CDF plotted in Figures 39 and 40 of the Appendix.

What this confirms is the large degree of variability in wind speed at any one fixed location through time. This means that it would be unreliable and therefore insufficient for a power grid to depend merely on the instantaneous real time supply from offshore

wind turbines without integrating storage solutions – such as pumped hydroelectric or lithium-ion batteries (Serat 2024).

It is also worth reemphasising the non-linear relationship – as per Equation 1 - between wind velocity and power output. Recalling that the mean wind speed of  $10.04 \left( \frac{m}{s} \right)$  of the sampled area generates  $4.9360 \left( \frac{MW}{turbine} \right)$ , if the wind speed is **decreased** by 10% to  $9.036 \left( \frac{m}{s} \right)$  - which is entirely typical as per Figures 39 and 40 – the new output power is found to be  $3.5983 \left( \frac{MW}{turbine} \right)$  as per Calculation 7 of the Appendix. This is a **27.1%** reduction in power output per turbine.

Similarly, if the wind speed is **increased** by 10% to  $11.044 \left( \frac{m}{s} \right)$  - which again is entirely typical as per Figures 39 and 40 – the new power output is found to be  $6.5698 \left( \frac{MW}{turbine} \right)$  as per Calculation 8 of the Appendix. This is a **33.1%** increase in power output per turbine.

---

### CHAPTER 3: COMPONENTS OF AN OFFSHORE WIND TURBINE

---

Whilst this report focusses on Jacket foundations, it is important to understand the full assembly of an offshore wind turbine. Figure 42 of the Appendix visualises the key components and the following text provides a description for each.

- A – **Hub**: Connects the blades to each other and to the main shaft, forming the rotor.
- B – **Nacelle**: The large metal shell at the top of the tower. This protects and houses the gear box, main shaft and generator amongst many other components.
- C – **Tower**: Acts as a structural column for the weight and dynamic forces of the rotor and of all components housed in the nacelle.
- D – **Blades**: Capture the kinetic energy from the velocity and mass of the wind and use this to rotate the main shaft and hence the generator.

**E.1 – Monopile Foundation:** As discussed in Chapter 4, a large cylinder that is driven into the ground; the most common foundation type in current UK offshore infrastructure.

**E.2 – Jacket Foundation:** The focus of this report – a welded truss style frame with three or four legs; as with the Monopile case, fixes the assembly into the ground and ensures its stability through both normal and extreme environmental conditions.

**F.1 – Rotor Brake:** Ceases the rotation of the rotor during high wind speeds, low wind speeds or for maintenance.

**F.2 – Yaw Brake:** Locks the nacelle into place stopping unwanted rotation once the turbine has been aligned with the wind.

**G – Yaw Actuators:** Orient the nacelle and rotor to face the wind directly, maximising power generation.

**H – Converter Cabinets:** Converts the non-synchronous power output [ $\neq 50$  Hz] of the generator into a grid compatible power [50 Hz].

**I – Transformer Room:** Takes a generator output of 600 (V) and increases this to 33,000 (V). The first of two voltage transformations; occurs in the Nacelle.

**J – Cooling Systems:** These regulate the temperature of critical components - for example, the generator, gearbox, converter cabinets and voltage transformers.

**K – Transition Piece:** A steel cylinder that connects the base of the tower to the top of the foundation; used in both the Monopile and Jacket case.

**L – Offshore Substation:** Takes the 33,000 (V) from the voltage transformation that occurs in the Nacelle and transforms this for a second time to 400,000 (V).

**M – Main Shaft:** The shaft that the hub and blade subassembly – the rotor - is fixed to.

**N – Gear Box:** Transforms the relatively slow rotational speed of the main shaft into a significantly larger rotational velocity.

**O – High Speed Shaft:** The output shaft of the gearbox; the shaft of the generator.

**P – Generator:** Induces the flow of electrons through oscillating electromagnetic interactions.

**Q.1 – Ultrasonic Wind Sensor:** Measures both wind speed and direction.

**Q.2 – Wind Vane:** Measures wind direction only. Used in parallel with the Ultrasonic Wind Sensor to provide two signals for direction to form a more reliable understanding.

Q.3 – **Anemometer**: Measures wind speed. As with the wind vane, this is used in parallel with the Ultrasonic Wind Sensor to provide two signals of speed to form a more reliable understanding.

---

## CHAPTER 4: FOUNDATION TYPES

---

Two foundation types are common in the UK. These are shown below in Figure 4.

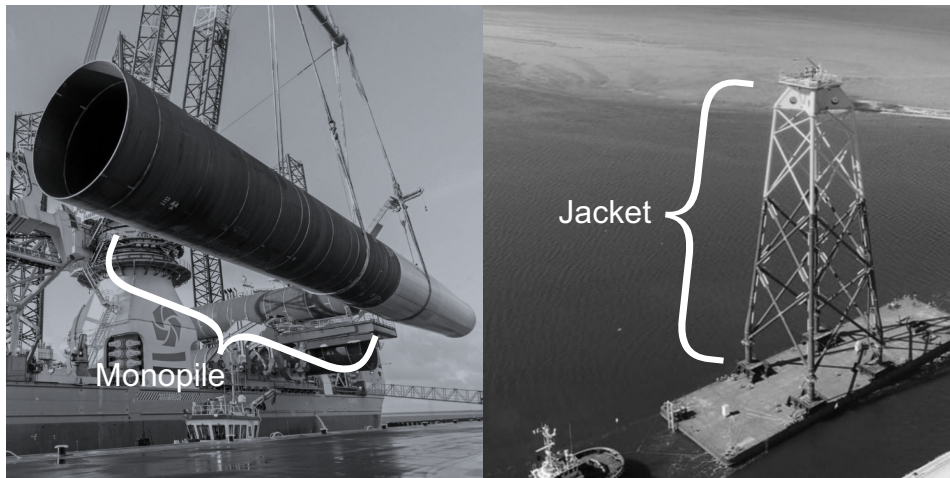


Figure 4: visualising the two common foundation types for Offshore Wind turbines.

Monopile foundations account for the overwhelming majority of the existing UK fleet at a prevalence of approximately 88.6% - with this being approximately 11.4% for Jacket foundations. As mentioned in Chapter 2, the third foundation type – cables tied to floating turbines – account for just 0.34% of the installed capacity worldwide (McCoy et al 2024).

Monopile foundations are large cylinders typically made out of S355 or S420 structural Steel (Mehmanparast et al 2018). They are typically 80 (m) in length and 10 (m) in diameter although naturally this is adjusted to suit the geotechnical conditions. The monopile gets driven in to the seabed by a powerful hydraulic hammer that rests on top of the monopile during its installation – see Figure 41 of the Appendix. Once installed the monopile acts as a structural column supporting the mass of the assembly above it.

Jacket foundations are large truss style frames with three or four legs and are made rigid by an assembly of welded tubular braces. They are also typically made out of S355 or S420 structural steel. The jacket foundation is secured to the seabed at its feet by piles which are – as with the monopile – driven by a now submerged hydraulic hammer. Both foundation types are prefabricated on land and then transported out to the site of installation by tug boat.

As discussed in Chapter 2, Monopile foundations are suitable for water depths of  $20 \leq d_{sea} \leq 40$  (m) while Jacket foundations are suitable for water depths of  $5 \leq d_{sea} \leq 50$  (m). This means that Jacket foundations have a greater depth range; however, Monopiles are still preferred in industry where possible due to their relative ease of installation. Monopiles require either a sand or clay seabed to survive piling. Jackets can be installed into seabeds of sand, clay and hard rock – making them more versatile. Where there is a hard rock seabed this will typically be predrilled before the piles are driven in.

---

## CHAPTER 5: MODES OF CONDITION MONITORING

---

It is imperative that society moves towards sustainable systems and structures to limit the use of raw materials. It is important therefore to ensure wind turbines not only last the 25 year design life but if possible beyond that timeframe.



Figure 5: from Left to Right – Fire in the Nacelle of an Offshore Turbine; Catastrophic Collapse of the Tower of an Onshore Turbine; Biofouling in the Jacket Foundation of an Offshore Turbine (Buck and Langan 2017).

The primary mode of avoiding premature failure is through sophisticated and informed design; this design stage optimisation has been to a large extent accomplished over the last 138 years of iteration – since Professor James Blythe’s original design in 1887 – shown in Figure 43 of the Appendix.

What matters now is being able to sense for unexpected and unusual emerging degradation, which to some degree is ineradicable, such that these individual components can be replaced before its failure cascades into a system wide catastrophe.

Naturally, this swapping of components is more applicable to the smaller units housed in the Nacelle, such as the Bearings, Gears, Shaft and Brake Pads. Replacing the tower or the foundation is, in most cases, unrealistic and instead would serve the purpose of protecting the healthy functioning components above them from also being lost. The sensing for emerging degradation of components within Engineering has been termed Condition Monitoring – where this is typically with reference to a rotating component. The aggregation of this understanding into the preservation of a full-scale macroscopic structure has been termed Structural Health Monitoring. However, as noted in (Worden and Dulieu-Barton 2004), in either case the Engineers are most fundamentally observing for emerging degradation such that there can be intervention and selective replacement or repair before the full system breaks down or its production is unnecessarily postponed.

There are three distinct sensors that form the cornerstones of Structural Health Monitoring; these are:

- **Strain Gauge:** measures transient deformation under novel loads by experiencing a change to resistance as a function of deformation.
- **Accelerometer:** measures changes in modality via piezoelectric crystals that experience known changes to voltage in response to their displacement.

- **Acoustic Emission:** witnesses crack propagation; as with the accelerometer, via piezoelectric crystals that experience known changes to voltage in response to their displacement.

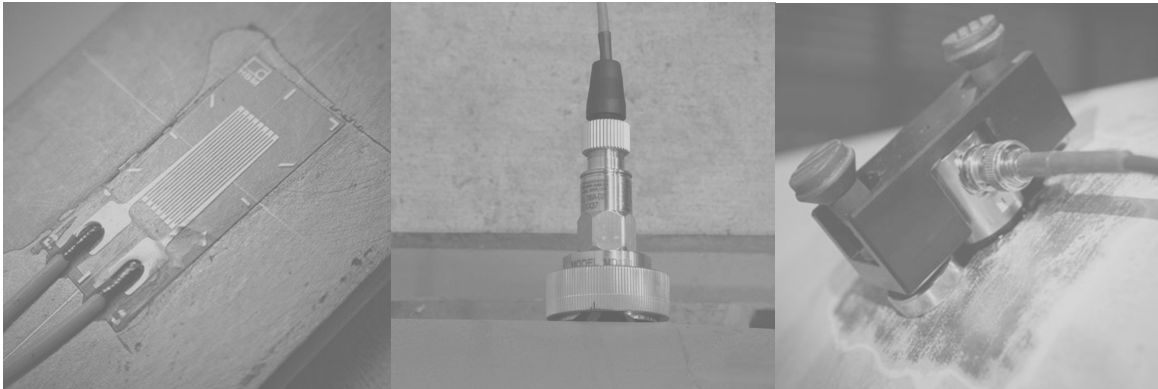


Figure 6: from Left to Right – Strain Gauge; Piezoelectric Accelerometer; Piezoelectric Acoustic Emission Sensor.

Together, these sensors allow Engineers to track strain, dynamic vibrational response and fracture – providing an holistic multi-modal understanding of emerging degradation before failure. The author's summer project will – as with last year's project (Cock 2024) – be focused on the Accelerometer.

## CHAPTER 6: TYPICAL FAILURE IN JACKET FOUNDATIONS

Actual catastrophic failure of these structures is exceedingly rare. Given that the existing infrastructure is overwhelmingly privately owned by for-profit publicly traded companies, the intellectual property surrounding the precise failure rate; its cause; its remedies, are fiercely guarded and sadly therefore disintegrated from the academic literature. However, a good proxy for this true rate of catastrophic failure can be taken from the privately owned but widely adopted DNV-ST-0126 standard for the Support Structures for Wind Turbines. In this widely adopted standard the stated threshold for acceptable rates of catastrophic failure is  $1 \cdot 10^{-4}$  per unit per annum – i.e., one in every ten thousand units per year, or 0.01%.

Focusing our attention on Jacket foundations exclusively, where failure does occur - and where the specifics of this have made their way into the academic literature - the failure has been due to:

---

**Mode 1 - Fatigue Cracking:** microcracks form at the grain boundaries between the crystals of a metal or about inclusions (a contamination of unintended chemistry) during loads that would otherwise manifest in elastic deformation. This most often occurs at the Jacket's welded joints due to their sharp geometry, irregular surfaces and a general loss of control over the crystallisation of the metal substrate during the welding process. This local plastic deformation then grows through thousands of cycles of loading – with no classically obvious signs of emerging degradation until, eventually, the crack reaches a critical length and a full fracture manifests – where this will be sudden and catastrophic.

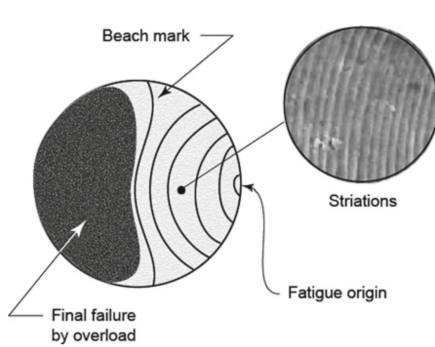


Figure 7: a diagram of the process of failing through Fatigue Crack formation (Milella 2024).

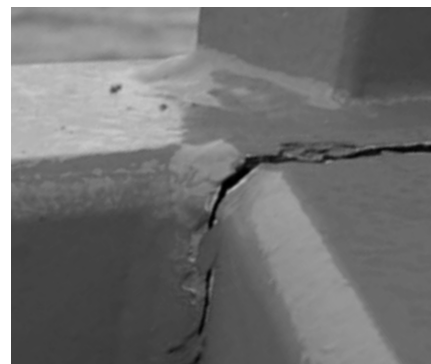


Figure 8: Fatigue Crack Failure of an Offshore Platform's Crane - not a Jacket foundation but the same failure mode and a strong example.

---

**Mode 2 – Corrosion:** generally speaking, chemical reactions fundamentally are the collision of previously disconnected atoms such that, with proper velocity and orientation, the geometry of the configuration of their electrons rearranges and the atoms become coupled; often with the rejection of a previously coupled atom.

In simple systems, such as two gaseous molecules colliding, this can be easily conceptualised. However, when corrosion occurs in a metal the reaction is more complex. There is still ultimately the collision between two previously disjointed molecules or atoms – in this case,  $O_2(g)$  from the air and  $H_2O(l)$  from the sea that has landed on the splash zone of the Jacket. The splash zone is the region of the Jacket exposed to both air and sea water.

However, unlike with conventional atomic collisions, electrons travel through the matrix of metal atoms of the Jacket from a separate volume of the Jacket. This process is known as electrochemistry – precisely because it involves the transmission of electrons through a metal matrix of atoms; where there are two distinct reactions occurring at either end of this transmission.

This cascades through a series of subsequent reactions that ultimately form rust and microcracks. The splash zones of both Monopiles and Jackets are coated specifically to avoid this phenomenon – however, if these coatings fail, corrosion will occur.

The corrosion occurs both beneath and at the splash zone. The corrosion under the splash zone typically emerges symbiotically with biofouling due to an increased asperity, such that organisms have an easier time latching on.

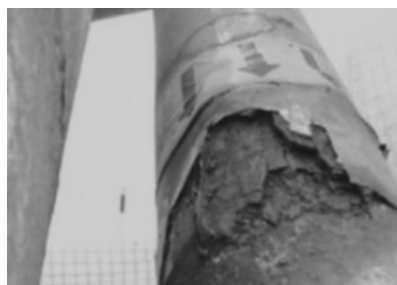


Figure 9: Corrosion of a Jacket Foundation (Zhang et al 2024).

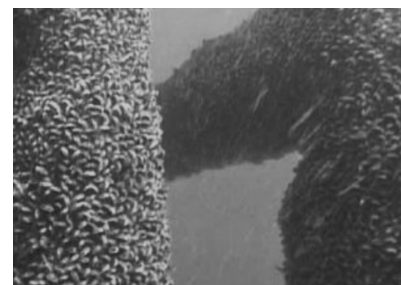


Figure 10: Biofouling of a Jacket Foundation (Barba 2017).

---

**Mode 3 - Seabed Erosion:** where the sand or clay about the top of the pile is gradually removed through time by the velocity of the adjacent volume of water. This is, naturally,